



FE Modeling of CFRP-Retrofitted RC Frames with Masonry Infill Walls

Mohamed A. Sakr^a, Saher R. El-khoriby^b, Ayman A. Seleemah^b, Essam A. Darwish^{c*}

^a Assoc. Prof., Department of Structural Engineering, Tanta University, Egypt.

^b Prof. of Structural Engineering, Department of Structural Engineering, Tanta University, Egypt.

^c Assistant lecturer, Department of Structural Engineering, Tanta University, Egypt.

Received 1 February 2017; Accepted 8 April 2017

Abstract

A number of numerical and experimental studies have been reported in recent literature to investigate the effects of infill walls on the seismic response of RC infilled frames. Many experimental studies used CFRP sheets as an external bracing system for retrofitting the infilled RC frames. It has been found that the common mode of failure of such retrofitted frames is the debonding of the CFRP-concrete adhesive material. In the current study, the behaviour of CFRP retrofitted infilled RC frames was investigated with a finite element micro model. In that model, a four-node shell element was used for modeling the concrete, infill panel and CFRP sheets. The interaction between concrete frame and infill panel was modelled using contact surfaces to allow the occurrence of separation and prevent penetration. Nonlinearities of the concrete, infill panel, steel and CFRP sheets were considered. To allow the occurrence of debonding mode of failure, the adhesive layer was modelled using cohesive surface-to-surface interaction model, which assumes that the failure of cohesive bond is characterized by progressive degradation of the cohesive stiffness, which is driven by a damage process based on the fracture energy. The proposed model was verified using experimental results from the literature. Results indicated that the cohesive model could capture the debonding mode of failure which has been observed experimentally. The validated micro model was used to investigate the effects of the strip end area, the anchor location and partial bonding of the CFRP sheet to the infill panel surface on the behaviour of infilled frames. The results of parametric study showed that, to get the highest efficiency of the CFRP retrofitted infilled frame, bonding about 25% only of the diagonal length from each end is sufficient to get the same behaviour of the totally bonded sheet.

Keywords: Infilled RC frames, CFRP Retrofitted, Finite Element Model, Debonding.

1. Introduction

Retrofitting of constructions vulnerable to lateral loads is a current problem of great political and social relevance. Many existing buildings are subjected to seismic action. Most of these buildings have ordinary non-ductile RC elements, beams and columns, infilled with brick walls (infilled RC frames). Many experimental works have been conducted to investigate the seismic behavior of partially infilled frames, infilled frames with opening, and retrofitted and unretrofitted infilled frames. Therefore, they represent conclusive scientific evidence for the possibility of using the infill walls as lateral load structural elements.

Hashemi and Mosalam [1] and Al-Chaar [2] investigated experimentally the behavior of infilled RC frames subjected to lateral loads. The results indicated that, the infilled RC frames exhibit significantly higher ultimate strength, residual strength, and initial stiffness than the bare frames. Furthermore, the number of bays appears to be influential with respect to the peak and residual capacity, the failure mode, and the shear stress distribution.

* Corresponding author: essam.darwish@f-eng.tanta.edu.eg

➤ This is an open access article under the CC-BY license (<https://creativecommons.org/licenses/by/4.0/>).

Kakaletsis and Karayannis [3] and Tasnimi and Mohebkah [4] investigated the influence of both masonry strength and openings on infilled RC and steel frames, respectively. They have proven that infill with openings can significantly improve the performance of RC frames. Further, specimens with strong infill exhibited better performance than those with weak infill.

Ozsayin et al. [5] studied 36 hollow brick wall specimens either under uniaxial compression or diagonal tension before and after retrofitting externally with CFRP sheets. They found a significant contribution of CFRP sheets to the mechanical characteristics of hollow brick walls in terms of several important structural design parameters such as Young's and shear modulus, axial and shears strengths as well as the deformation capacity.

Sinan et al [6] investigated the strengthening of masonry infilled RC frames using diagonal CFRP strips under cyclic loads. They investigated the effects of CFRP strips' width and arrangement type on specimens' behavior, strength, stiffness and story drifts of the test specimens. They proved that, the diagonal CFRP strips significantly increased both the lateral strength and stiffness.

Erdem et al. [7] investigated experimentally the behavior of two different techniques for strengthening RC infilled frames. One of the frames was strengthened with RC infill. While the other frame was strengthened with CFRP strengthened hollow clay blocks. The test specimens were subjected to reversed cyclic quasi-static loading. Strength, stiffness, and story drifts of the test specimens were evaluated. They proved that both strengthened frames behaved similarly under cyclic loading.

Yuksel et al. [8] presented the behavior of bare, infilled, and carbon fiber reinforced polymer CFRP retrofitted infilled RC frames with different bracing configurations. The test results showed a significant increase in the yield and ultimate strength capacities of the frames with a decrease in relative story drifts. The energy dissipation capacities of the retrofitted frames turned out to be more than those of the unretrofitted infilled frame, thus reducing the seismic demand imposed on the frames.

Chen and Yeh [9] studied the out-of-plane seismic behavior of reinforced concrete (RC) frames infilled with brick walls. The test results showed that the contribution of the brick walls to the out-of-plane lateral strength of frames was not straightforward, although the residual strength of frames infilled with brick walls was clear. Retrofitting enhanced the peak lateral and residual strengths in tested specimens.

Many researchers have studied the effects of masonry panels on RC frames, in order to propose and validate some analytical approaches that are able to evaluate the contribution of panels to the local and global behavior of structures. Different approaches have been developed to analyze the behavior of masonry infilled frames. The modeling strategies of infilled frames can be classified into micro- and macro-modeling, based on the detail by which they represent an infill wall, the computational effort and the information they provide about the behavior of a structure. Micro-models are used to reproduce and analyze the local behavior with great detail and require long computational time in the case of models with a large number of elements. Macro-models, on the other hand, reproduce the global behavior of a structural element, giving results in terms of stiffness and strength with relatively low computational time.

According to FEMA356 [10], the elastic in-plane stiffness of a solid unreinforced masonry infill panel prior to cracking shall be represented with an equivalent diagonal compression strut.

Fiore and Netti [11] showed that single strut models can provide an adequate estimation of the stiffness of infilled frame, but cannot be used to obtain realistic values of bending moments and shear forces in frames. They proposed a new approach by dividing the calculated width equally between the two non-parallel struts, which is able to take into account the local effects. Asteris et al. [12] proposed a reduction factor able to take the effect of openings in an infill panel to calculate the effective width.

On the Micro-modeling level, Alam et al. [13] constructed micro models to analyze retrofitted and unretrofitted masonry-infilled RC frames under in-plane lateral loading. A 2D plane stress elements was used. The frame and the wall are connected by interface elements that are capable of transferring normal and shear stresses. The adopted numerical model was fairly accurate in estimating the ultimate load carrying capacity of the retrofitted infilled frame.

D'Ayala et al. [14] modeled the infill panel as a homogenous material where the effects of the bricks and mortar are smeared into a continuum referred to as a 'meso' model. They also showed that the simulation of the panel behavior with a more generic tool than the compressive strut is critical to the correct interpretation of the load paths through the composite structures.

Doudoumis [15] investigated analytically the effects of the alternative modeling of the interface conditions, the density of discretization mesh, the size of friction coefficient, the relative beam-column stiffness, the relative frame-infill size and the orthotropy of the infill panel are evaluated. It is concluded that all these modeling parameters considerably affect the behavior of the examined infilled frames, except for the parameter describing the infill's orthotropy. Asteris [16] proposed a criterion to describe the frame-infill separation. The basic characteristic of this analysis is that the infill-frame contact lengths and the contact stresses.

Asteris et al. [17] presented a general classification scheme of the failure modes of infilled frames. Such a classification of failure modes improves substantially the understanding of the earthquake resistant behavior of infilled frames and leads to better methodological approaches regarding their modeling, analysis and design.

Using finite element modeling, Nwofor and Chinwah [18] investigated the contribution of openings in masonry infill panels on the reduction of the shear strength of infilled frames. It was concluded that, the model was effective in wind and seismic vulnerability analysis of reinforced concrete infilled frames with openings. Nwofor [19] constructed a numerical model using explicit finite element method to study the behavior of masonry infilled reinforced concrete frames. He compared obtained results against results from experimental test to ensure the ability of his model to stimulate the shear strength response of masonry infill panel.

Mohyeddin et al. [20] introduced a detailed presentation of a generic three-dimensional discrete-finite-element model that has been constructed to model reinforced-concrete frames with masonry infill using ANSYS. A simple method was proposed to overcome convergence issues which are related to the Newton–Raphson algorithm. Dehghani et al. [21] used engineered cementitious composite (ECC) to strengthen infilled RC frames. Erol [22] investigated seismic strengthening of non-structural brittle masonry infill walls of RC frames by CFRP. Kakaletsis [23] made a comparison of CFRP and alternative seismic retrofitting techniques for bare and infilled RC frames. Another research presented a technique for strengthening of reinforced concrete infilled frames with textile-reinforced mortar (TRM) jacketing [24]. Strepelias et al. [25] experimentally investigated the behavior of concrete frames infilled with RC for seismic rehabilitation. Akin [26] studied the effects of various parameters on CFRP strengthening of infilled RC frames.

At the numerical analysis level, many researchers studied the behavior of infilled frames using either micro- or macro-models. For example, Akin et al. [27] performed a numerical study on CFRP strengthening of reinforced concrete frames with masonry infill walls. These numerical methods achieved good agreement with the experimental work, providing strong tools to study the behavior of infilled frames, whether the overall behavior using macro-models or the local behavior using micro-models.

As described later in the literature review, many studies reported experimentally the results and benefits of infilled frames for the seismic behavior of structures, as well as the benefits of CFRP strengthening for the infilled frames to increase their in-plane shear capacity and dissipated energy. The observed CFRP debonding failure mode is considered an obstacle to achieve the maximum benefit from the high resistance of the CFRP materials.

To the author knowledge, there is no previous numerical study on modeling the behavior of CFRP retrofitted infilled frames, capable of simulating the debonding mode of failure and crack progress through the adhesive layer. The current study aims to fill this gap. In this study, the behavior of CFRP retrofitted infilled RC frames was studied numerically using a finite element 3D shell model. The interaction between concrete frame and infill panel was modeled. Nonlinearities of the concrete, infill panel, steel and CFRP sheets were considered. To allow the occurrence of debonding mode of failure, a cohesive surface-to-surface interaction model was used to model the adhesive layer. This interaction model assumes that the failure of cohesive bond is characterized by progressive degradation of the cohesive stiffness, which is driven by a damage process based on the fracture energy.

2. Finite Element Analysis

The finite element analysis package ABAQUS/standard [28] was used to model a CFRP retrofitted infilled RC frame. A brief description of the constitutive models that are used in the model is presented below. Figure 1. illustrates the components of the CFRP retrofitted infilled frame.

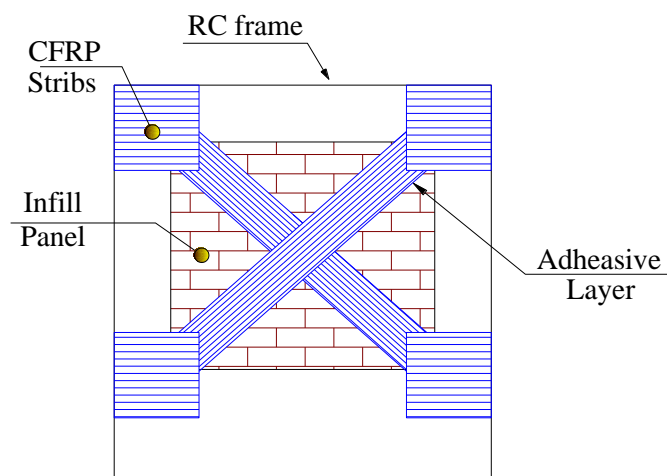


Figure 1. Components of the CFRP retrofitted infilled frame

2.1. Constitutive models

The concrete damage plasticity model was used to model the concrete behaviour. This model assumes that the main two failure modes are tensile cracking and compressive crushing [28]. The elastic parameters required to establish the tension stress-strain curve are elastic modulus, E_c , and tensile strength, f_{ct} . According to the (ACI 318-99) [29] E_c and f_{ct} were calculated. To specify the post-peak tension failure behaviour of concrete, the fracture energy method was used. For the uni-axial compression stress-strain curve of the concrete, the stress-strain relationship proposed by Saenz [30] was used. To specify the post-peak tension failure behaviour of concrete, the fracture energy method was used, as shown in Figure 2, where the fracture energy, G_f , is the area under the softening curve.

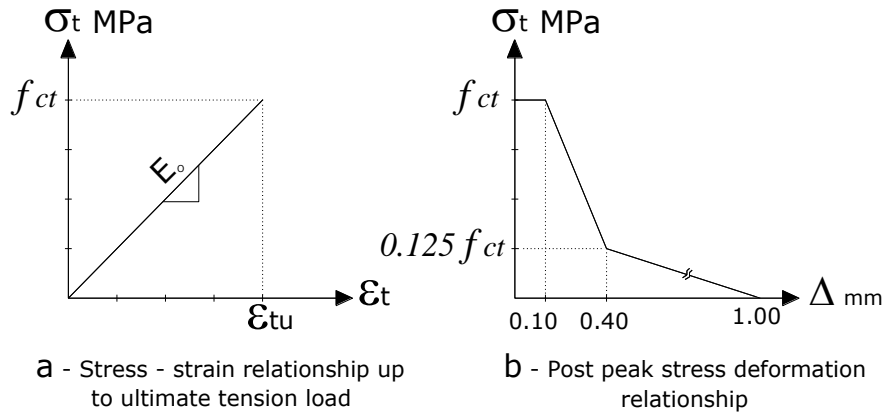


Figure 2. Concrete behavior for uniaxial tension

The steel was assumed to be bilinear elastic-plastic material identical in tension and compression. The "concrete damage plasticity model" was used to model the infill panel, as shown in Figure 6. The CFRP material was considered as linear elastic isotropic until rupture [31].

2.2. Interaction between Concrete Frame and Infill Panel

Experiments have shown that under lateral forces, the concrete frame tends to separate from the infill near windward lower and leeward upper corners of the infill panels, causing compressive contact stresses to develop between the frame and the infill at the other diagonally opposite corners, in addition to the transverse component which represent the shear stress. ABAQUS/standard provides a node-to-node interaction method using Cartesian connector element. Cartesian connector element provides a connector between two nodes that allows independent behaviour in the three local Cartesian directions. To define the Cartesian connectors' properties in the present model, the normal and tangential mechanical behaviour must be defined. For the normal behaviour, an elastic-plastic connector was used. To prevent the connector element of transmitting the tension force, a Force/Moment failure criteria has been defined. The tangential behaviour was defined using the penalty friction formulation with a friction coefficient equal to 0.25 as specified in [11].

2.3. Interface between CFRP strips and the infilled frame surface

The interface between CFRP strips and the infilled frame surface was constructed using a cohesive interface by the traction separation law to allow for the debonding failure mode, Figure 3. The available traction-separation model assumes initially linear elastic behaviour followed by the initiation and evolution of damage.

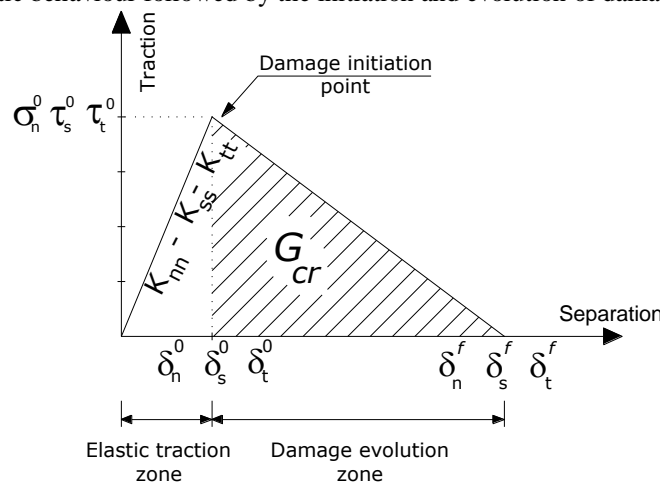


Figure 3. Description of the traction-separation behavior [26]

Surface-based cohesive behaviour which is primarily intended for situations in which the interface thickness is negligibly small, can be used to model the delamination at interfaces directly in terms of traction versus separation in the three local directions; the normal and the two shear directions of the surface. It assumes that the failure of cohesive bond is characterized by progressive degradation of the cohesive stiffness, which is driven by a damage process [32]. The interface thickness is considered negligibly small, and the initial stiffnesses K_{nn} , K_{ss} , and K_{tt} , in the normal and two shear directions, respectively, are defined as [31, 33]:

$$k_{ss} = k_{tt} = \frac{1}{\frac{t_i}{G_i} + \frac{t_c}{G_c}} \tag{1}$$

where t_i is the resin thickness, t_c is the concrete thickness, and G_i and G_c are the shear modulus of resin and concrete, respectively, and E_i and E_c are the modulus of elasticity of the resin and concrete, respectively. The upper limit for the maximum shear stress τ_{max} was provided by Obaidat et al. [34].

Damage initiation refers to the beginning of degradation of the cohesive response at a contact point. The process of degradation begins when the contact stresses and/or contact separations satisfy certain damage initiation criteria. Maximum stress criterion was used which assumes that, the initiation of damage occurred when the maximum contact stress ratio (as defined in the expression below) reaches a value of one. This criterion can be represented as:

$$\max \left\{ \frac{\sigma_n}{\sigma_n^o}, \frac{\tau_s}{\tau_s^o}, \frac{\tau_t}{\tau_t^o} \right\} = 1 \tag{2}$$

Where σ_n^o , τ_s^o , and τ_t^o represent the peak values of the contact stress when the separation is either purely normal to the interface or purely in the first or in the second shear direction, respectively. And σ_n is the cohesive tensile stress and τ_s , and τ_t are the cohesive shear stress in the two perpendicular directions s and t .

From Figure 3, it is obvious that the relationship between the traction stress and effective opening displacement is defined by the elastic stiffness, K_{nn} , K_{ss} and K_{tt} , the local strength of the material, σ_n^o , τ_s^o and τ_t^o and the energy needed for opening the crack, G_c which is equal to the area under the traction–displacement curve.

Interface damage evolution was expressed in terms of energy release. The description of this model is available in the ABAQUS material library [32]. The dependence of the fracture energy on the mode mix was defined based on the Benzaggah–Kenane fracture criterion[32].

Benzaggah–Kenane fracture criterion is particularly useful when the critical fracture energies during deformation purely along the first and the second shear directions are the same [31]; i.e. $G_s^c = G_t^c$. It is given by:

$$G_n^c + (G_s^c - G_n^c) \left\{ \frac{G_s}{G_T} \right\}^\eta = G^c \tag{3}$$

Where $G_s = G_s + G_t$, $G_T = G_n + G_s$, and η is a cohesive property parameter.

2.4. Elements and Meshing

Four-node doubly curved thin or thick shell, reduced integration, finite membrane strains (S4R) was used for modelling the concrete, infill panel, CFRP sheets. While a 2-node linear 3-D truss (T3D2) element was used for modelling the reinforcement steel. A sensitivity analysis was carried out to get the optimum mesh size. The optimum meshes size it is illustrated in Table 1. The bond between steel reinforcement and concrete was assumed as a perfect bond.

Table 1. The approximate mesh size used in the model

Part	Element Type	Approximate mesh global size (mm)	Boundary Conditions
Concrete	A 4-node doubly curved thin or thick shell, reduced integration, hourglass control, finite membrane strains.	30	According to Figure 5.
RFT steel	A 2-node linear 3-D truss	40	
Infill Panel	A 4-node doubly curved thin or thick shell, reduced integration, hourglass control, finite membrane strains	Min. 15 and Max. 30	
CFRP sheets	A 4-node quadrilateral membrane, reduced integration, hourglass control.	Min. 8 and Max. 25	

3. Verification of the Model with Previous Work

Experimental data was obtained from previous work by Yuksel [8]. This experimental study focused on the behaviour of bare and CFRP retrofitted infilled RC frames with different bracing configurations. Quasi-static experimental results were presented and discussed for six 1/3-scaled infilled RC frames that were retrofitted using CFRP material in various schemes. The cross bracing retrofitting scheme was selected to perform that study. The dimensions and RFT details of the infilled frame are shown in Figure 4 and 5. shows the pre-loads, configuration and dimensions of Yuksel cross-braced retrofitted infilled frame.

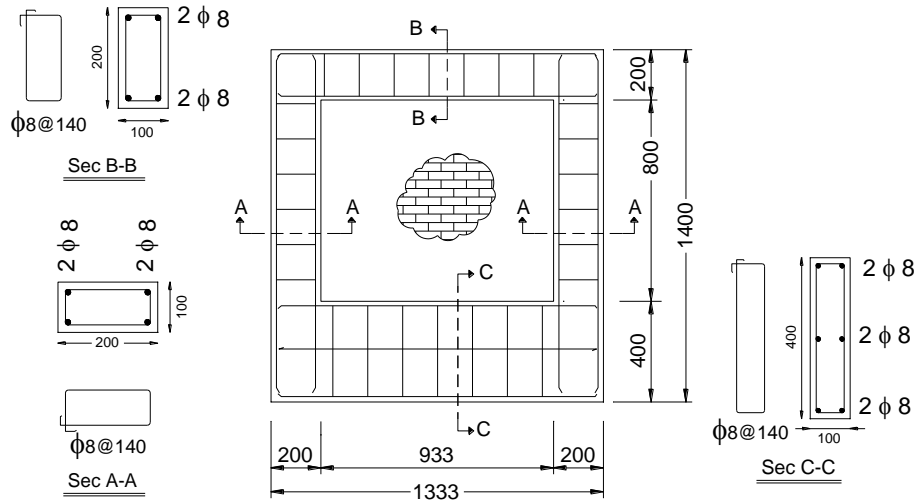
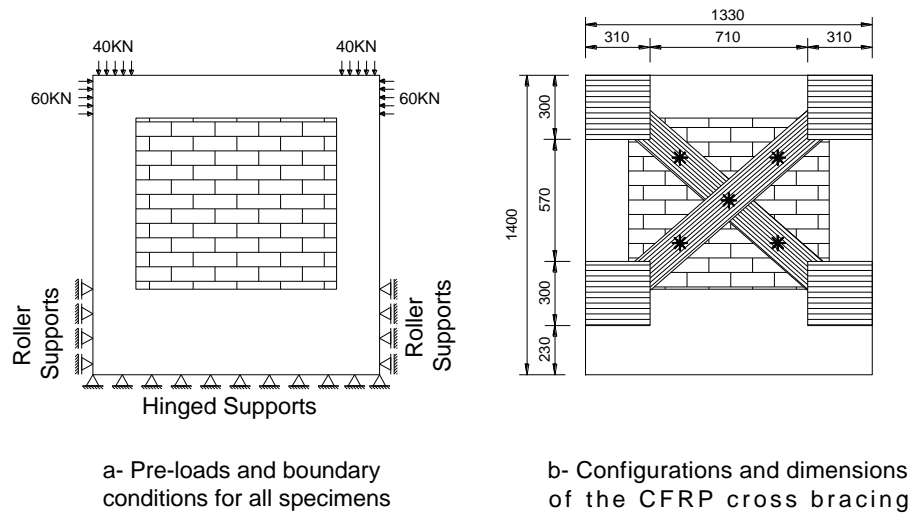


Figure 4. Dimensions and RFT details of Yuksel infilled frame [8]



a- Pre-loads and boundary conditions for all specimens

b- Configurations and dimensions of the CFRP cross bracing

Figure 5. (a)-Pre-loads and boundary conditions, (b)- Configuration and dimensions of Yuksel cross-braced retrofitted infilled frame [8]

3.1. Material Properties and Applied Loads

The compressive strength, $\bar{\sigma}_c$, was, in the experimental work, 19 MPa. E_c and σ_{ct} were then calculated according to Figure 2. Poisson's ratio for concrete was assumed to be 0.20. For the RFT steel, the elastic modulus, E_s , and yield stress σ_y , was in the experimental work for the main steel and stirrups $E_s = 209$ GPa and $\sigma_y = 420$ MPa and $\sigma_u = 500$ MPa. A Poisson's ratio of 0.3 was used.

The infill panel was represented as an isotropic material, the average compressive strength of the infill panel was assumed to be 4.14 MPa as the average of the two directions' compressive strengths and the Elastic modulus was taken 7000 MPa. Tensile strength for the concrete masonry used in the referenced experimental work was not provided, and as it is usually a parameter subjected to relatively high uncertainty, especially for low engineered masonry infilled frames, a conservative failure value of 0.65 N/mm² for tensile cracking was used [14]. To specify the post-peak tension failure behaviour of concrete masonry, the fracture energy method was used. Many trials have been carried out to find the optimum value of the fracture energy of infill and were found to equal 422 J/m, Figure 6.

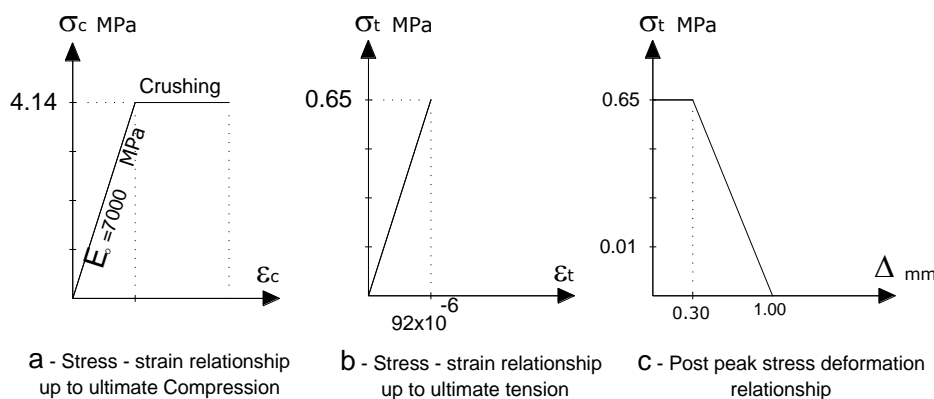


Figure 6. Stress–strain relationships for an infill panel

According to [8], the fiber density is $1.79 \times 10^5 \text{ N/mm}^3$. Also, the modulus of elasticity of the CFRP is 230 GPa and the tensile strength and ultimate elongation capacities are 3900 MPa and 1.5%, respectively. The width of strip is 150 mm and its thickness is 0.165 mm. It was bonded to the surface using epoxy resin.

The values used for the resin thickness t_i is 1 mm, and the concrete thickness t_c is 5 mm, $G_i = 0.665 \text{ GPa}$, $G_c = 10.8 \text{ GPa}$, $E_i = 2.5 \text{ GPa}$, $E_c = 20487 \text{ MPa}$. A value of 2.00 MPa was used for the maximum shear stress, τ_{\max} . For the maximum normal stress, it was taken equal to the concrete tensile strength with a value of 2.00 MPa. For the fracture energy, G_{cr} in the two shear directions, previous researches have indicated values from 300 J/m^2 up to 1500 J/m^2 [34]. Different values were used in the current verification. These values are 100 J/m^2 , 300 J/m^2 , 500 J/m^2 , 700 J/m^2 . The value used for the fracture energy G_{cr} in the normal direction equals 100 J/m^2 [34]. In the experimental work, the specimens were subjected to unidirectional cyclic lateral loading under 40 kN constant axial load, representing 10% of the column's axial load bearing capacity, applied on each column. The actuator was fixed to the specimen by using two post-tensioned rods of 20 mm in diameter producing approximately 60 kN axial force on the beam, Figure 5 [8]. The envelopes of lateral load versus story drift displacement cycles are given in the reference work of Yuksel [8], which represent the pushover curves of the bare frame (BF), infilled frame (IF) and CFRP retrofitted infilled frame (RF). This can be used for verifying the finite element model under monotonic lateral load with the experimental work. Automatic stabilization and small time increment were also used to avoid a diverged solution.

3.2. Bare and infilled frame (BF - IF)

The Lateral load vs. lateral drift curves obtained for bare and infilled frames from experimental and FEM analysis are shown in Figure 7. Also, Figure 8. demonstrate the yielding zones of the longitudinal RFT in the bare and infilled frames, respectively. Figure 9 and 10. compare between the modes of failure of the bare and infilled frames. The analysis shows a good agreement between FEM and experimental results, the error in predicting the ultimate load in the IF model was about 4.20%. The good agreement indicates that the constitutive models used for concrete and reinforcement can reasonably capture the mechanical behaviour.

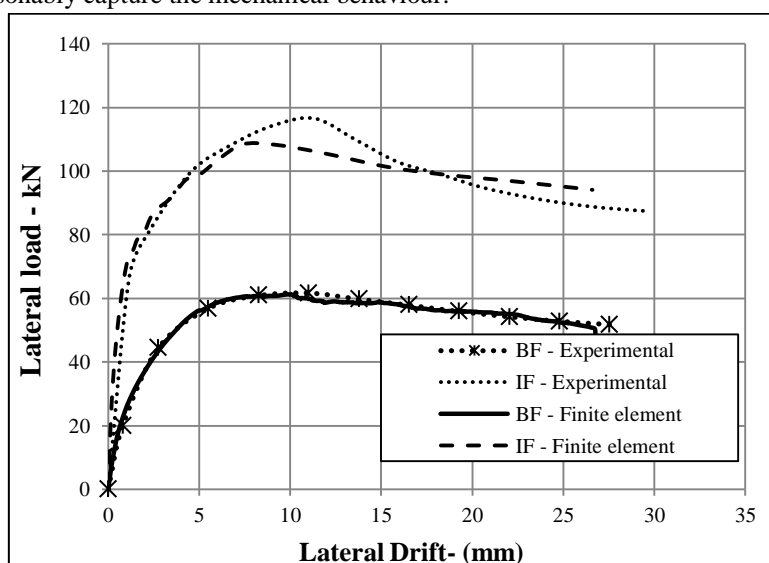


Figure 7. Lateral load vs. story drift curve for bare and infilled frames

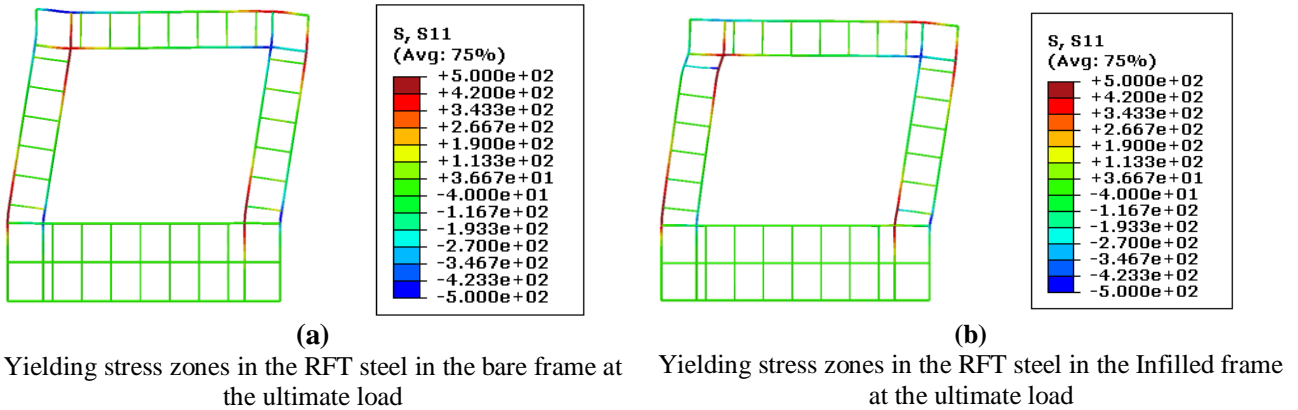


Figure 8. Yielding stress zones in the RFT steel in the bare and infilled frames

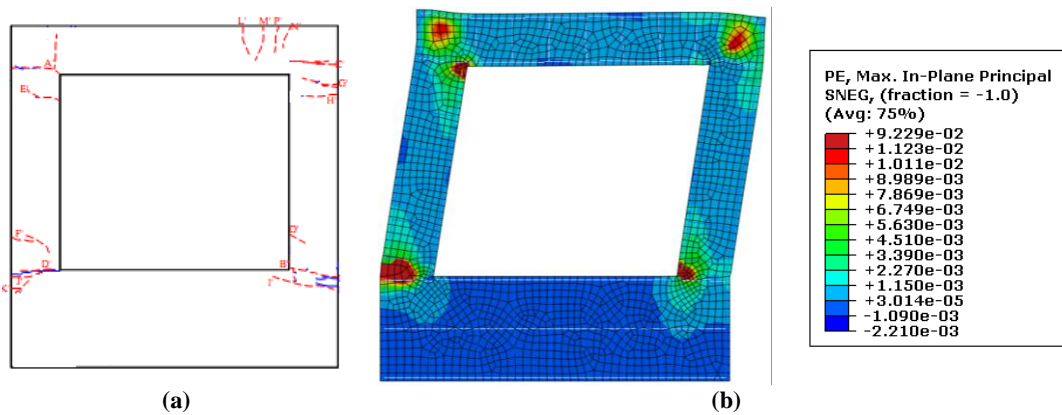


Figure 9. Modes of failure and crack survey - (a) Damage pattern for bare frame (Experimental [8]) – (b) Plastic strain pattern represents cracks (Finite element)

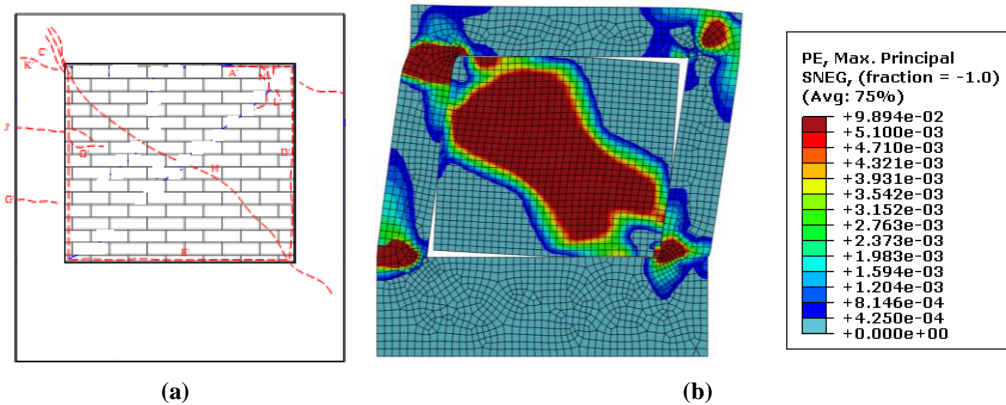


Figure 10. Modes of failure and crack survey - (a) Damage pattern for infilled frame (Experimental [8]) - (b) Plastic strain pattern represents cracks (Finite element)

3.3. Cross Braced CFRP Retrofitted Infilled Frame

The CFRP-concrete interface surface was modelled using cohesive interaction ($RF-G_{cr} = XX$) with different fracture energy values, where the symbol XX refers to the fracture energy value. It is very important to notice that, in the experimental work, the CFRP was installed on the both faces of the infilled frame. The 3D shell model doesn't allow installing the CFRP on both faces of the shell element. So the stiffness, strength, fracture energies and also the CFRP sheet thickness values were multiplied by two, and then the CFRP was installed on one face.

Lateral load vs. lateral drift curves

The Lateral load vs. lateral drift curves obtained for the CFRP retrofitted infilled frames from experimental and

FEM results with full bond and different values of the fracture energies are shown in Figure 11. The initial stiffness of the models was close to experimental result. The stiffness of the adopted finite element models at intermediate loading varied slightly from the experimental results, Figure 11. For the cohesive models with different fracture energy values, matching of the four models was observed up to the debonding of each individual case. After debonding, the retrofitted frame behaved as an infilled frame. Increasing the fracture energy value leads to delay of the occurrence of debonding, and thus increases the ultimate load and the corresponding story drift, Figure 11.

The full bond model overestimates the stiffness at the intermediate loading stage, and also the ultimate load of the retrofitted infilled frame compared to cohesive models. This is due to the fact that the perfect bond does not take into consideration the shear strain between CFRP sheets and the installation surface. The full bond models fail to capture the softening of the retrofitted frame. Between the previous finite element models, the cohesive model with fracture energy equal 500 J/m^2 show good agreement with the experimental results. The error in predicting the ultimate load in the IF model was about 4.00%.

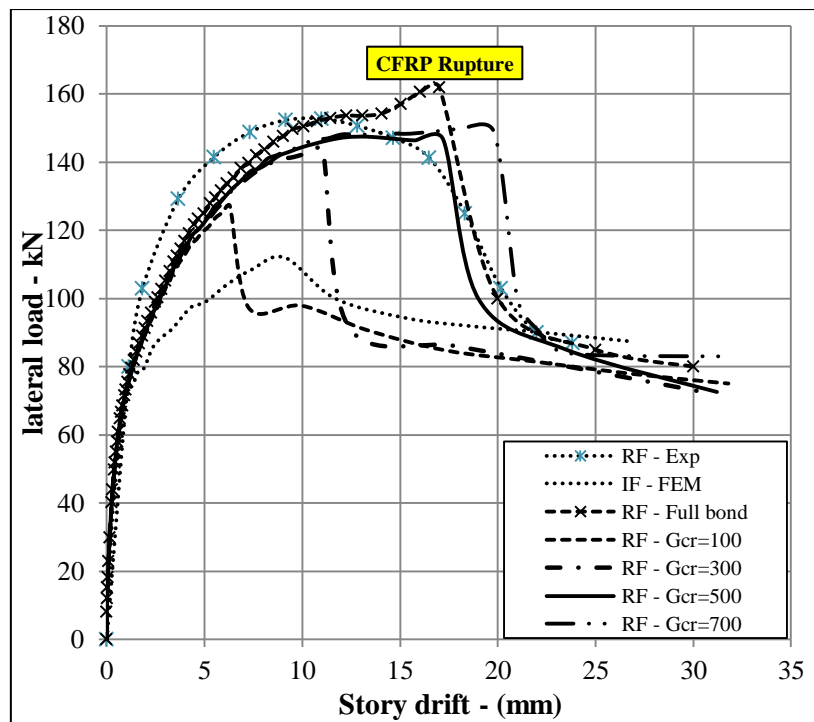


Figure 11. Lateral load vs. story drift obtained for the CFRP retrofitted infilled frames

Failure Modes

The assumption of full bond between CFRP and concrete is unable to model the debonding fracture mode, on the other hand, when the cohesive bond model was used, debonding fracture occurred, just like in the experiments. This is illustrated in Figure 12 and 13.

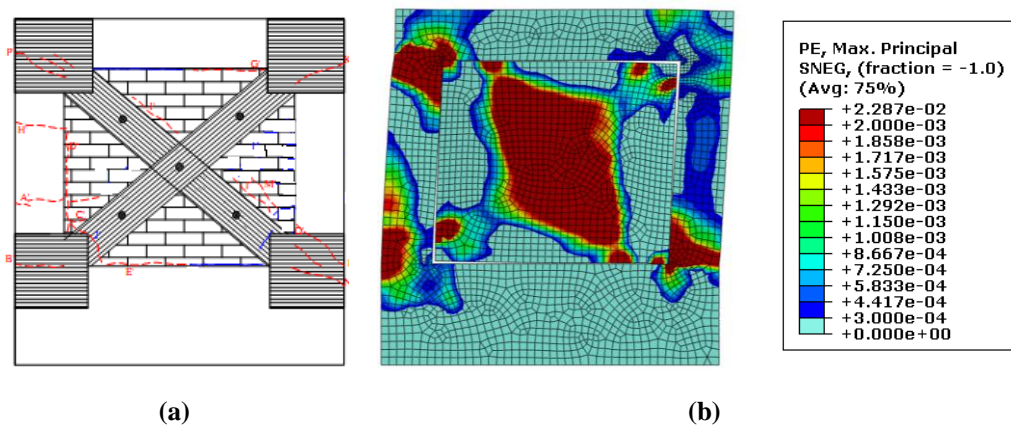


Figure 12. Modes of failure and crack survey - (a) Damage pattern for CFRP retrofitted infilled frame (Experimental [8]) - (b) Plastic strain pattern represents cracks (Finite element)

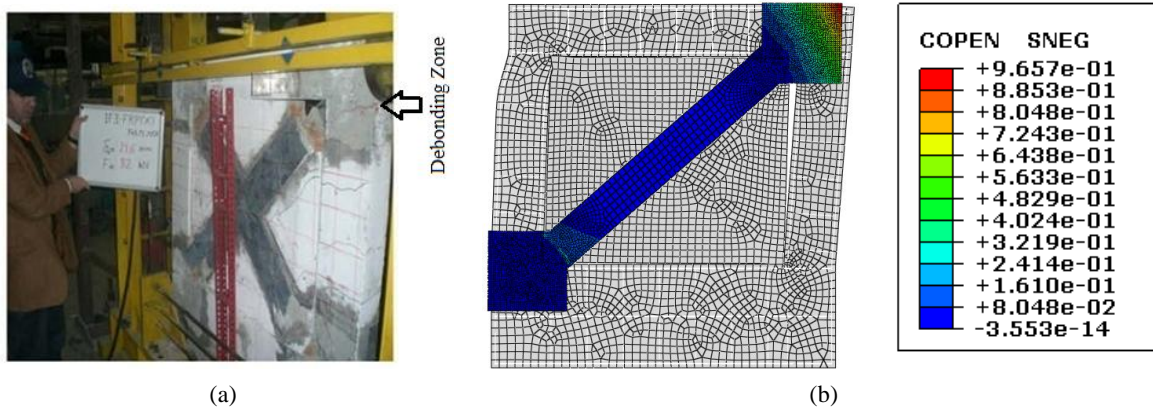


Figure 13. Debonding zones of CFRP sheets (a) experimental [8] (b) finite element analysis (contact open at surface nodes)

Stress in the bond layer

Debonding of CFRP is likely to initiate at the stress concentration in the bond layer, which occurs either at the end of the plate or at any intermediate crack. In the first case, it is called end plate debonding mechanism, where in the second case; it is call intermediate crack debonding mechanism. In the infilled frames, the occurred gap between the concrete frame and the infill panel can play the role of the intermediate crack where the debonding may occur, as shown in Figure 14. and 15. These figures indicate the transfer of shear stress at the interface layer from the beginning of debonding up to a complete failure. It is very important to notice that not all the interface area is effective, but only the area nearby the separation point. When it failed by debonding, the stress relocates to the neighboured non stressed zone up to complete failure, Figure 14.

With the beginning of loading and up to a load of 87 KN, the debonding begins at the point of maximum shear stress concentration near the gap, Figure 14. (1-8). By increasing the load gradually after the initiation of debonding, a transition of maximum shear stress to neighbouring points occurs up to the end of the CFRP sheet. From Figure15, it was observed that the shear stress zone on the infill panel surface doesn't transfer, as the max shear stress cannot reach the strength value. In other words, no damage has occurred. On the other hand, the shear stress at the concrete surface transferred up to complete debonding, resulting in the occurrence of failure.

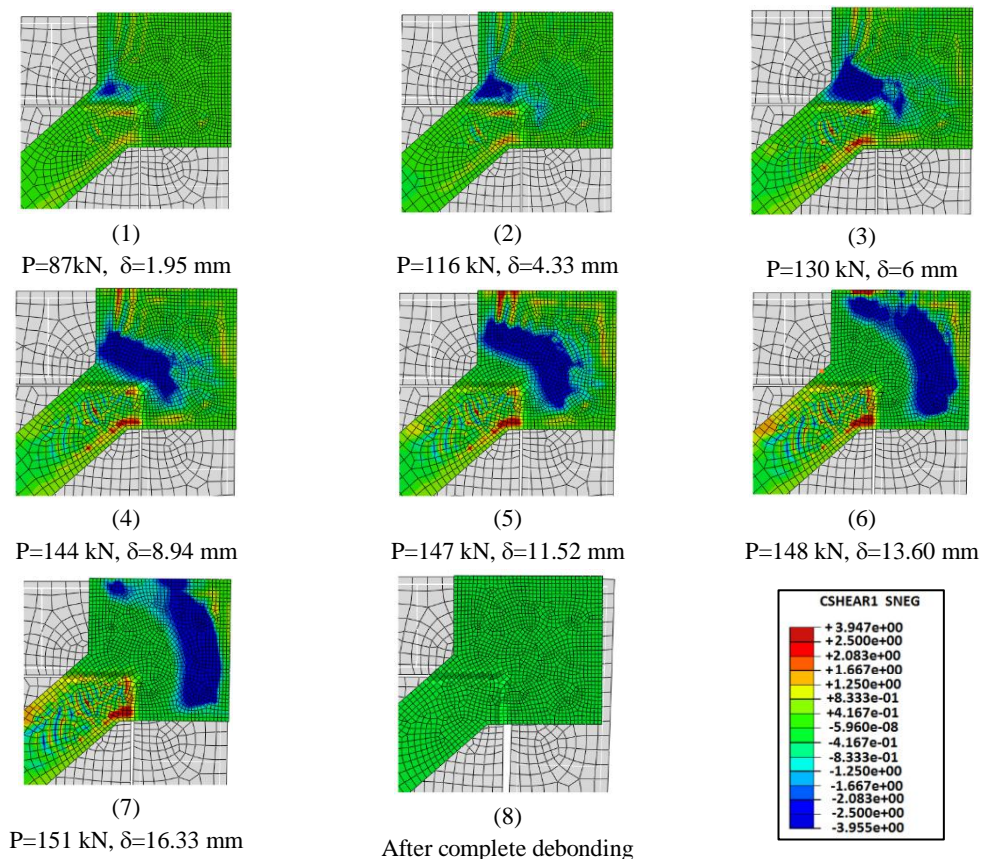


Figure 14. Transfer of the shear stress from the start of debonding up to complete failure

It was also noticed that the stress range illustrated from -3.95 MPa up to +3.95 MPa, as the shear strength which equals 2.00 MPa was multiplied by two to get the effect of the two surfaces on just one surface of the shell element.

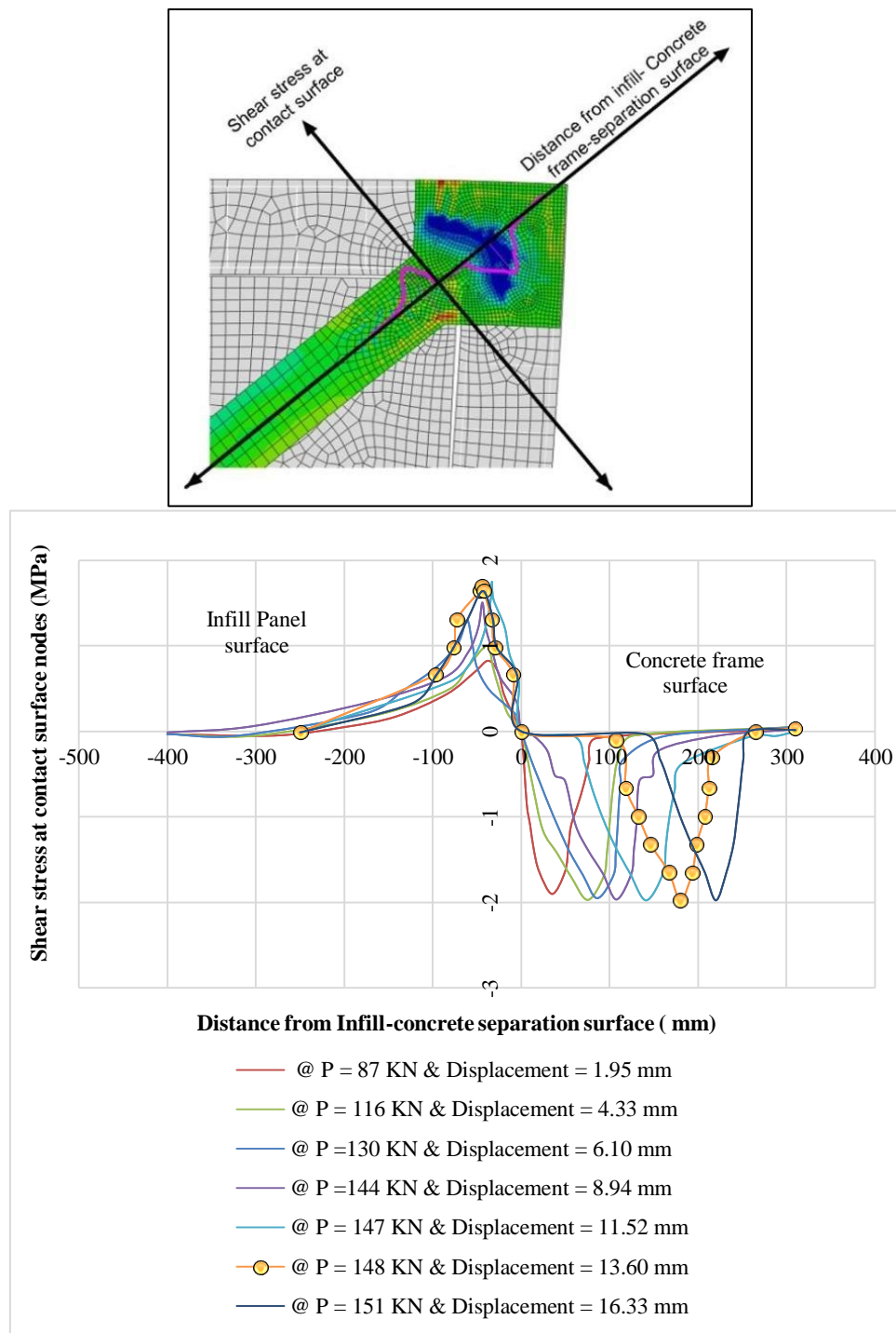


Figure 15. Transfer of the shear stress at different loads and its corresponding displacement

4. Parametric Study

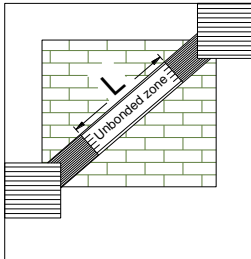
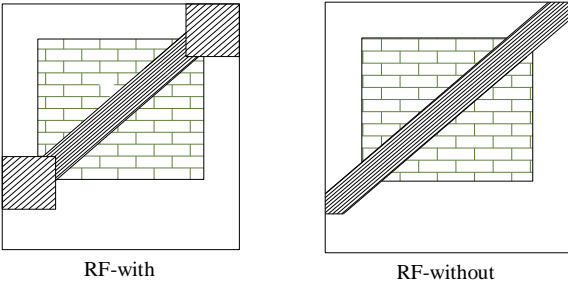
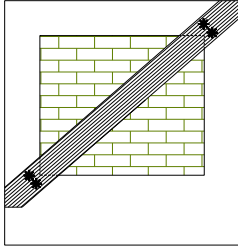
To investigate some of the factors which could affect the transfer of shear stress at the bond layer, three different parameters have been studied. These parameters are:

1. Partial bonding of the CFRP sheets to the infill panel surface.
2. Effect of the end supporting sheets on the ultimate load.
3. A proposed CFRP anchor location, based on the transfer of shear stress at the bond layer, to delay the debonding.

Symbolic meanings and configuration of the different parameters are summarized in Table 2. The value of the

adhesive layer fracture energy used in all next parameters is constant and equal to 500J/m².

Table 2. Symbolic meaning and configuration of different parameters

NO	Symbolic meaning	Configuration
1	Partial bonding of the CFRP sheet to the infill panel surface with unbounded length "L" (RF-UB-L).	
2	Effect of the end supporting sheet on the behavior of CFRP retrofitted cross braced infilled frame (RF-with) and (RF-without)	
3	Proposed location of anchors to delay the debonding (RF-A)	

4.1. Partial bonding of the CFRP Sheet to the Infill Panel surface

The cross bracing CFRP retrofitted infilled frame of Yuksel [8] was reanalysed, but in the presence of a new variable which is the unbonded length (L), as shown in Table 2. The unbonded length varied as 300 mm, 600 mm, 850 mm, and totally unbonded. Figure 16. shows a complete convergence between the behaviour of the reference model RF-G_{cr}=500 totally bonded, and RF-UB-300, and RF-UB-600 models. But there is a slight difference in the behaviour of RF-UB-850, and RF-UB-Totally.

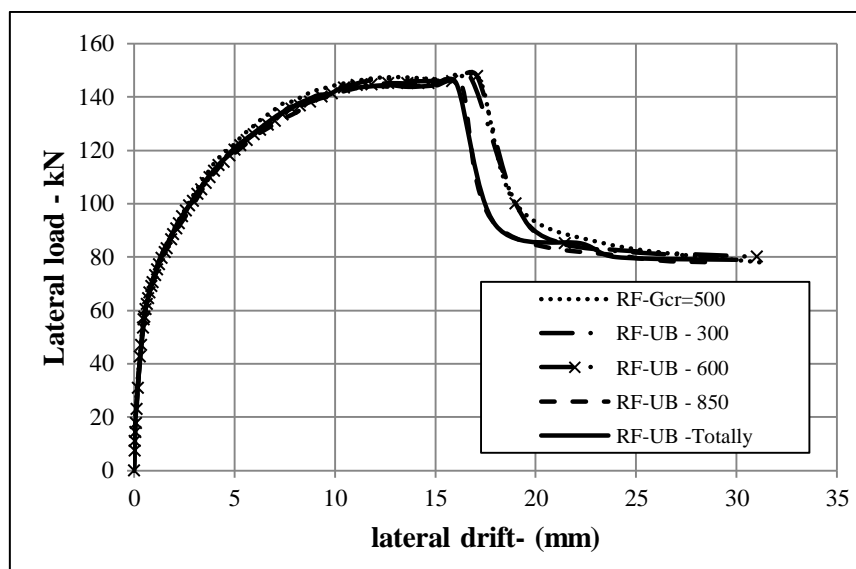


Figure 16. Lateral load vs. lateral drift obtained for (RF-Gcr=500) and (RF-UB-L) with different unbonded length

The first group, (RF- $G_{cr}=500$ totally bonded, RF-UB-300, and RF-UB-600) achieved almost the same debonding load 150 kN at the same story drift of 17.00 mm. The second group, (RF-UB-850 and RF-UB-Totally) achieved a maximum debonding load about 147 kN, which is slightly less than the debonding load value of the reference model, at a lateral drift equal to 16.00 mm. The stiffness is considered fully identical in all stages of loading.

From that result, the minimum bonding length of the CFRP sheet on the infill panel to get the same behavior of the totally bonded model was about 25% of the infill panel diagonal length. Decreasing that length will slightly affect the ultimate behaviour. Installing the CFRP sheet on a part of infill panel surface, about 25% of diagonal length, leads to delay of the onset of separation between the frame and infill wall, this delays the debonding process. By observing the values of the stresses generated on the wall in Figure 15, one can found that the stress didn't reach the shear strength value on the whole contact surface and that it is concentrated near the gap between the concrete frame and the infill panel and don't transmit to neighbouring areas, i.e. a small length of about 25% of the diagonal length is sufficient to maintain that balancing. This, together with the experimental observation shown in Figure 13 (a), confirms the correctness of the obtained results. Figure 17. illustrates the contact shear stress at the ultimate load for different debonding length. It is clear that, the bonded length on the infill panel surface has almost a negligible contact shear stress compared to that on the concrete frame surface.

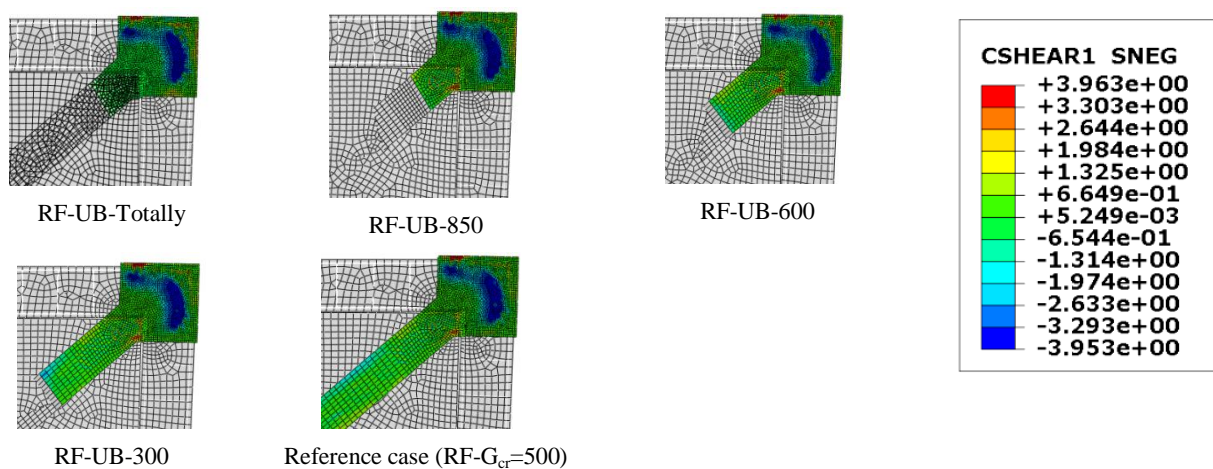


Figure 17. Contact shear stress for different models at the ultimate load

4.2. Effect of the end supporting sheet on the behavior of CFRP retrofitted cross braced infilled frame

With reference to Figure 5, the experimental cross bracing retrofitting system includes a square end supporting CFRP sheet bonded at the end of the CFRP strip. CFRP retrofitted infilled frame without this square sheet having the same mechanical and geometrical properties of the CFRP strip was modelled, as shown in Table 1.

Figure 18. illustrates the lateral load vs. lateral drift of the new proposed retrofitted infilled frame. The additional square part has a great effect on the retrofitted frame response. The original retrofitted frame (RF- $G_{cr}=500$) has an ultimate debonding load about 148 kN, while the frame without the square part (RF-without) has about 138 kN, i.e. the decrease in the ultimate load was about 6.75%, Figure 19 (a).

The ability of a structure to dissipate the seismic input energy is an accurate measure of its expected seismic performance. The amount of dissipated energy is determined as the area enclosed by the load-displacement curve up to a certain displacement or drift ratio [8]. The dissipated energy vs. lateral drift relations for the two models is shown in Figure 19 (b). The amount of dissipated energy of the two models at 1.0% drift ratio is the same, as no debonding has occurred yet. At 1.5% and higher drift ratios, RF- $G_{cr}=500$ dissipates higher energy due to the delay of debonding, Figure 19 (b).

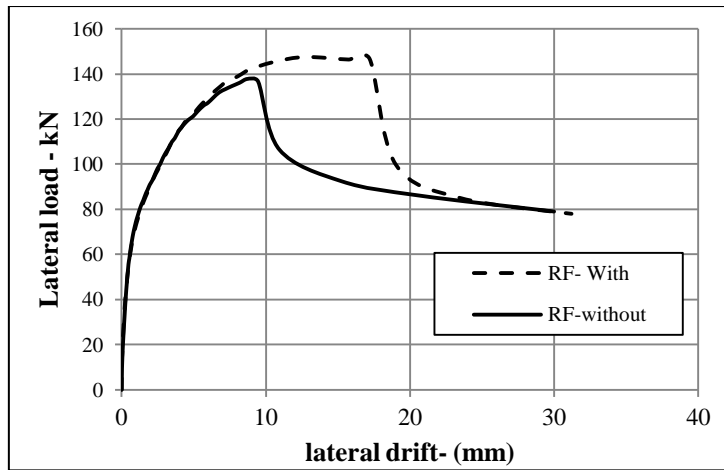


Figure 18. Lateral load vs. lateral drift obtained for strip configuration parameter

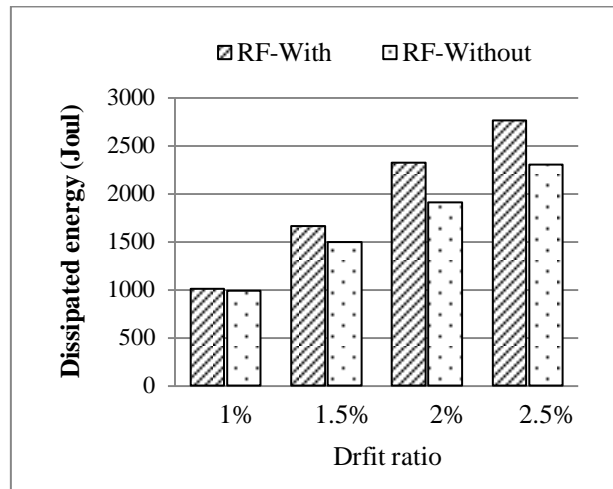


Figure 19. Change in the dissipated energy

The dissipated energy in the debonding failure is the contact area multiplied by the fracture energy needed to make a complete debonding. With reference to Figure 14 and 20, which illustrates the contact area at a different lateral load levels, the area which have the contact shear stress near the capacity of the surface for RF-Without is smaller than that of RF-With which leads to a significant reduction in the dissipative energy. Therefore, the amount of energy needed to cause a complete debonding in RF-Without is less than that needed in RF-with.

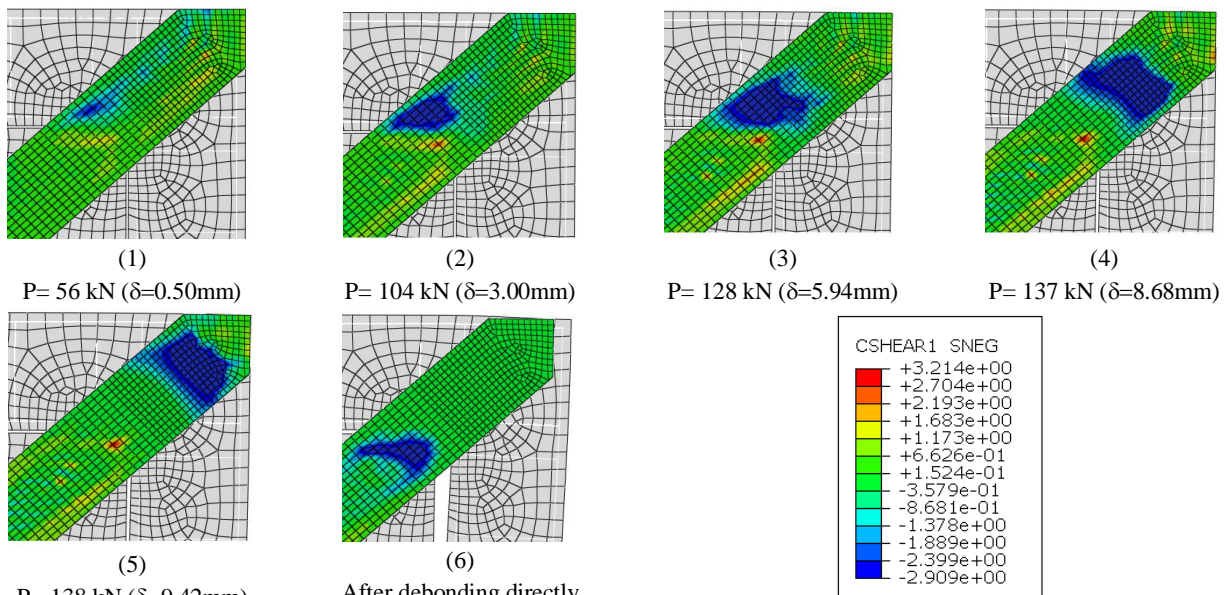


Figure 20. Contact shear stress between CFRP and concrete surface at different load levels for RF-Without at the top right corner

4.3. Proposed Location of Anchors to Delay the Debonding

The tension stresses that can be developed in CFRP sheets bonded to concrete represent only a fraction of the rupture strength of the sheet due to the premature failure by debonding. In order to make CFRP strengthening applications more efficient, a ways to anchor the sheets should be proposed so that failure by debonding was precluded. Various ways of anchoring the CFRP sheets to concrete have been investigated by researchers, including the use of transverse sheets or straps, using mechanical anchors, wrapping the end of sheets in rods embedded in grooves formed into the concrete , or using CFRP anchors [35].

Laboratory investigations performed by Niemitz et al. [36] indicated three primary FRP anchor failure modes: FRP anchor splay delamination, FRP anchor shear rupture, and FRP anchor pull out. FRP anchor delamination is a failure mode that occurred between fibres forming the anchor splay and the FRP sheet surface. FRP anchor shear rupture consists of anchor failure just below the FRP sheet surface, while the splay remained attached to the upper face of the FRP sheet. FRP anchor pull out was not a common failure mode and occurred only in the cases where insertion holes in the concrete were perhaps improperly cleaned.

In order to model the mechanical representation of the CFRP anchor response, Sergio et al. [35] proposed force-deformation relationship for modeling the CFRP anchors for shear rupture failure mode. They proposed two types of CFRP anchors, the first type was 13 mm anchor diameter with 51 mm splay diameter, where the second type was 19 mm anchor diameter and 102 mm splay diameter, as shown in Figure 21. The tension behavior of the anchor is the axial tension strength of the CFRP sheet used to make the anchor.

In order to convert this force-displacement behavior to a traction separation behavior, the elastic traction separation behavior was defined, and then the initiation of damage, and finally damage evolution part, Figure 22. (with reference to Figure 3).

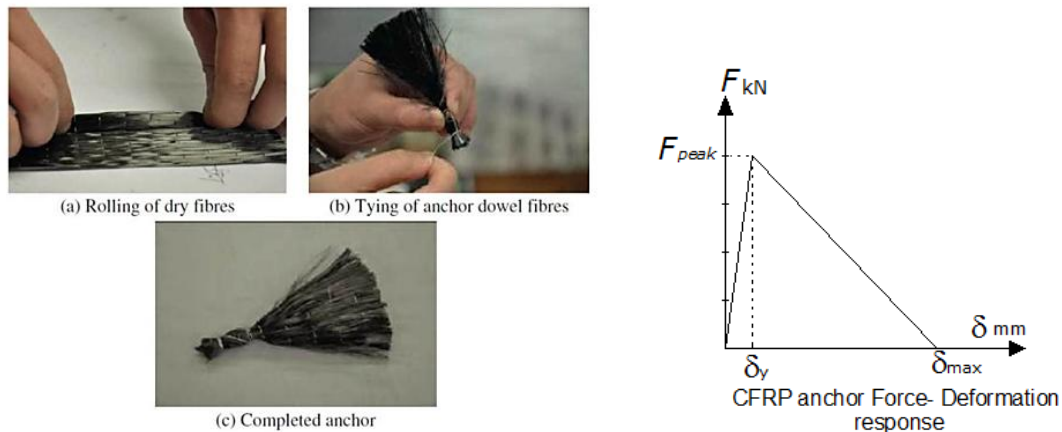


Figure 21. Proposed force-deformation relationship for the modeling of the CFRP anchors [30]

For damage evolution, the maximum displacement criteria was used instead of the maximum dissipated energy where $\delta_{max} = 1.78$ mm.

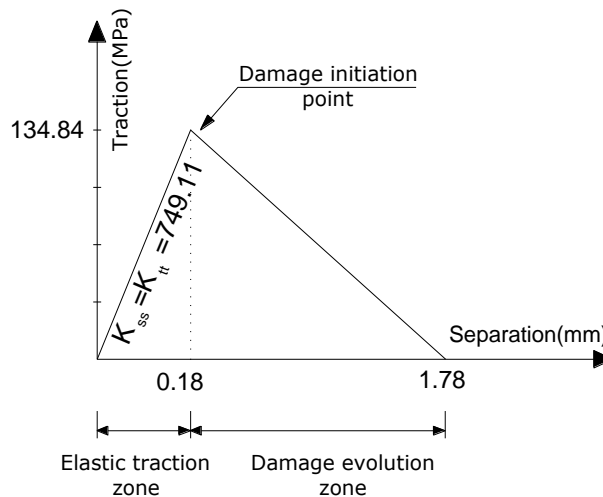


Figure 22. Traction separation behavior of the CFRP 13 mm anchor

Observing the transfer of contact shear stress in Figure 15, it can be anticipated that, by preventing the transfer of shear stress at the onset of debonding, a delay of the complete debonding can be achieved. Therefore, an anchor location at the point of maximum shear stress is proposed to delay the debonding mode of failure. Two anchors were used in the CFRP retrofitted frame without the end supporting sheet, RF-Without, near each end of CFRP strip at the shown distances, Table 1. The choice of that distance was selected to guarantee a sufficient concrete part to prevent concrete spalling.

For the RF-A-13 mm model, using the discussed anchor mechanical properties, the behavior was greatly improved comparing with the case of RF-Without in which no anchors were used, Figure 23. The location of debonding changed from the upper right corner to the lower left corner after the damage of anchors, Figure 24.

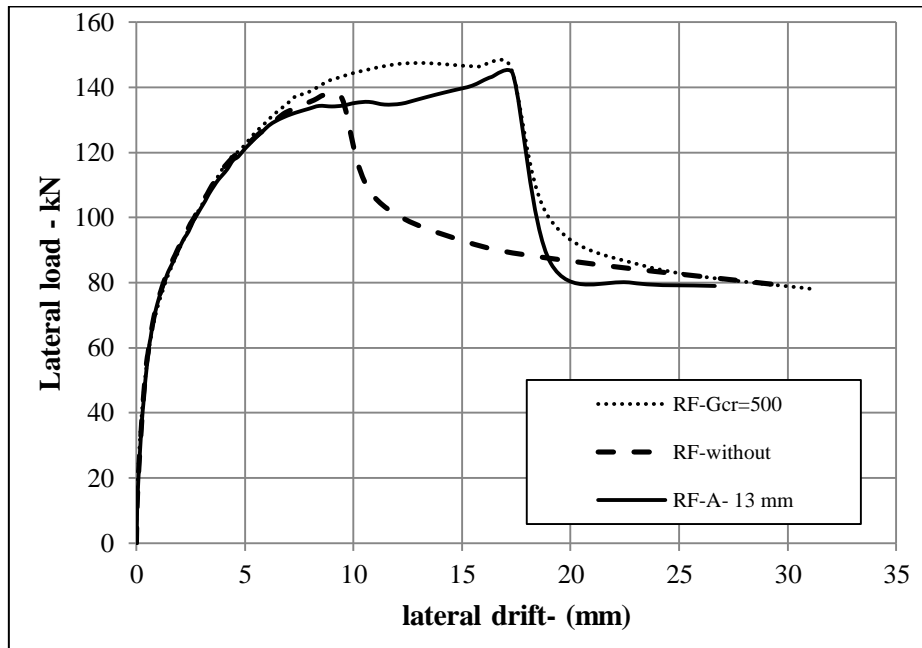


Figure 23. Lateral load vs. lateral drift obtained for RF-A-13 mm model

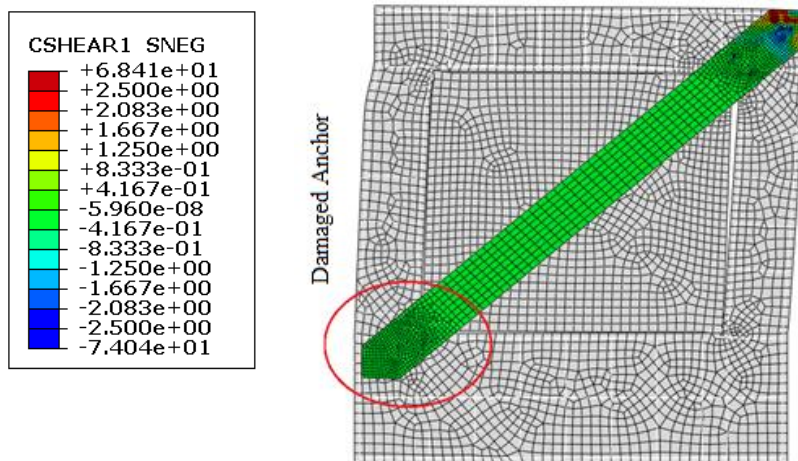


Figure 24. Mode of failure for RF-A-13 mm anchor (Anchor shear rupture)

From Figure 23, It was noticed that there is no significant increase of the ultimate load (137 kN vs. 144.4 kN), and there is a significant increase of the corresponding displacement (8.70 mm vs. 17.33 mm). This indicates that, using four 13 mm anchors increased the ductility by about 100% which is very useful in case of seismic event. The amount of dissipated energy is determined as the area enclosed by the load-displacement curve up to a certain displacement or drift ratio. The dissipated energy versus lateral drift relation for all models is given in Table 3. Up to drift ratio of 1.0%, the dissipated energy is almost the same for the three models, as the CFRP sheet is fully bonded to the infilled frame surface. By increasing the drift ratio over 1.5%, the occurrence of debonding in RF-XX model was reached, where the other two models are still without debonding.

Table 3. Dissipated energy for RF-A models at different drift ratios

Model	Dissipated energy at 1.0% drift (J)	Dissipated energy at 1.5% drift (J)	Dissipated energy at 2.0% drift (J)	Dissipated energy at 2.5% drift (J)
RF-G _{cr} =500	1003	1660	2318	2763
RF-A-13 mm	993	1601	2233	2630
RF-without	988	1495	1908	2298

The transfer of contact shear stress at the debonding zones is illustrated in Figure 25. at different load and displacement stages for the lower left corner where the debonding occurred. It is clear that the debonding started near the gap between the infill panel and the concrete frame, and then the shear stress reached the capacity at that point and dropped to reach zero and transferred to the adjacent zones. As the CFRP anchor permits some relative deformation between the upper and the lower components, it allowed the transfer of shear stress behind it up to the end of the sheet, while it was still carrying its loading capacity. By the increase of lateral load and consequently the story drift, the connection reached to debonding by the anchor shear failure, Figure 25. The stages of contact shear stress at the upper right joint are also shown in Figure 26.

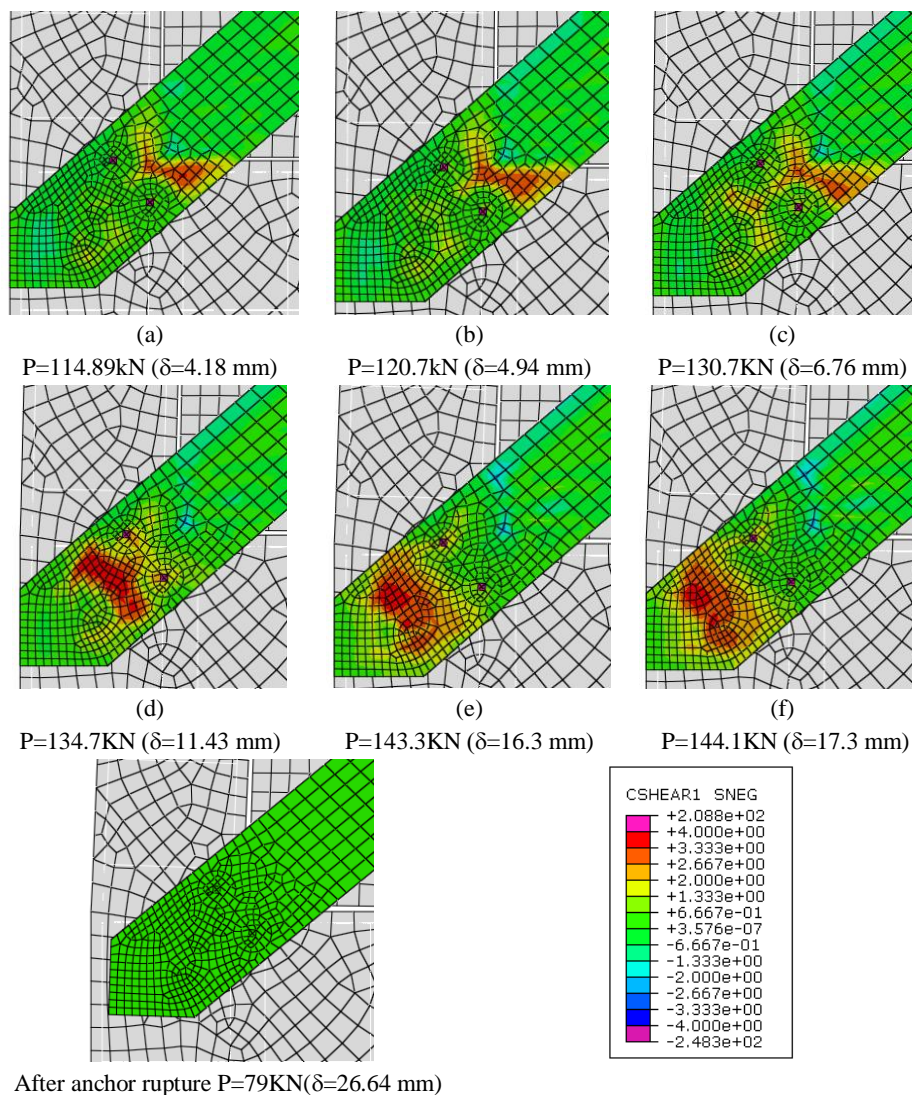


Figure 25. Transfer of the shear stress from the start of debonding up to complete failure at lower left joint for RF-A-13 mm

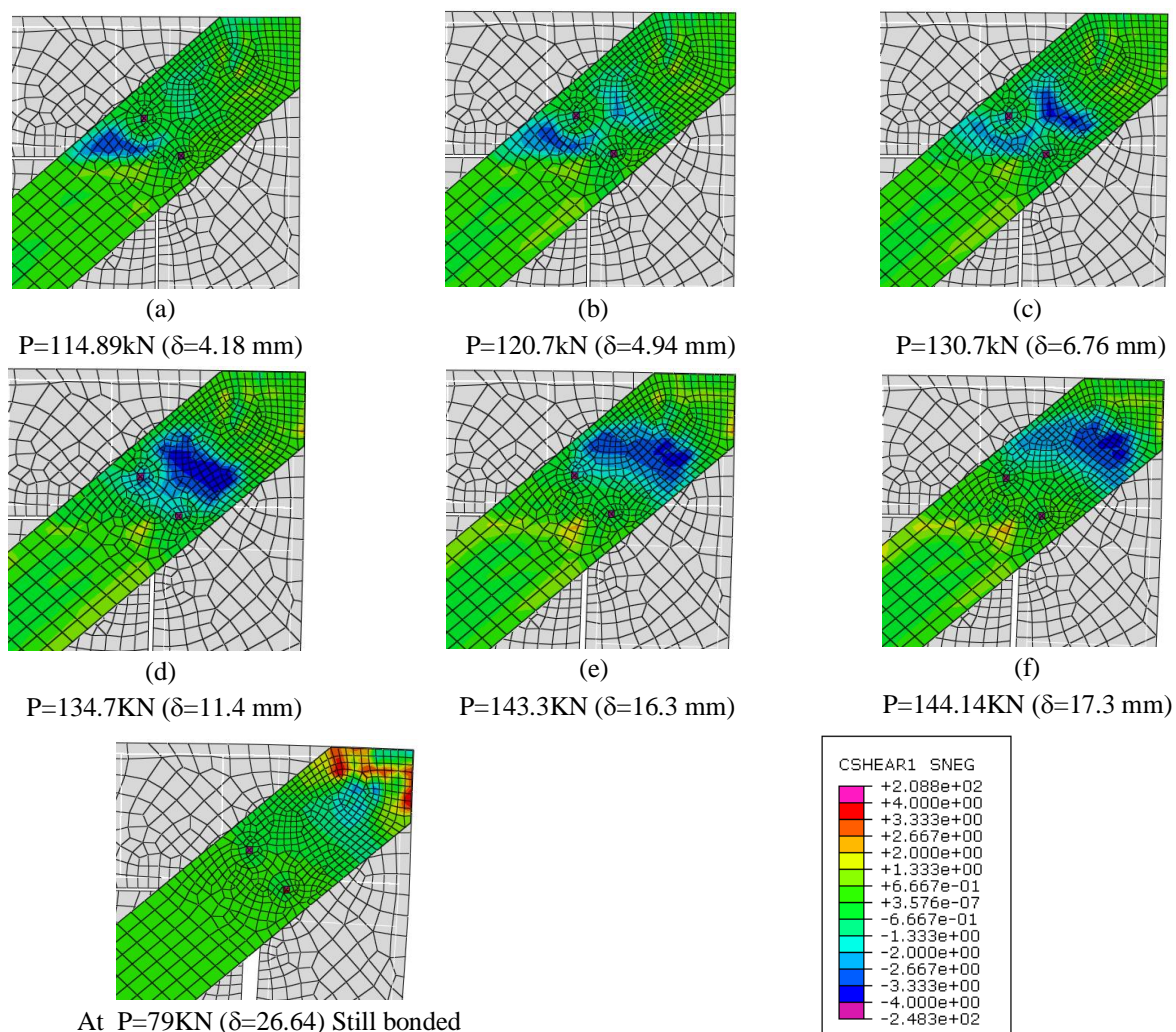


Figure 26. Transfer of the shear stress from the start of debonding up to complete failure at upper right joint for RF-A-13 mm

5. Conclusion

In this study, the behaviour of CFRP retrofitted infilled RC frames was studied numerically using a finite element 3D shell model. The interaction between concrete frame and infill panel was modelled. Nonlinearities of the concrete, infill panel, steel and CFRP sheets were considered. To allow the occurrence of debonding mode of failure, a cohesive surface-to-surface interaction model was used to model the adhesive layer. Based on the results, the following conclusions can be drawn:

- The assumption of perfect bond model can't represent successfully the CFRP infilled frame behaviour. On the other hand, the cohesive models have the same pattern of collapse as in the experimental work. The value of fracture energy of the adhesive layer gave a different collapse point whether for the collapse load or for the lateral displacement at the debonding point, which resulted in different values of ductility and dissipated energy.
- Partial bonding of the CFRP sheet to the infill panel surface has a little effect on the overall behaviour of the CFRP retrofitted infilled frame. The results showed that, to get the highest efficiency of the CFRP retrofitted infilled frame, bonding about 25% only of the diagonal length from each end is sufficient to get the same behaviour of the totally bonded sheet. So, determination of the fracture energy of adhesive layer should be accurately estimated.
- The increase of the CFRP strip end area with end supporting sheets has a positive effect on the overall behaviour of the CFRP retrofitted infilled frame. It results in increasing the ultimate load and the dissipated energy.
- By identifying the position of the maximum contact shear stress, the perfect place of CFRP anchors can be located to increase the capacity of retrofitted frame. Modelling the CFRP anchor must be capable of representing the mode of failure of the real anchor.

6. References

- [1] Hashemi A, Mosalam KM. Shake-table experiment on reinforced concrete structure containing masonry infill wall. *Earthquake Engineering & Structural Dynamics*. 2006;35:1827-52.
- [2] Al-Chaar G, Issa M, Sweeney S. Behavior of Masonry-Infilled Nonductile Reinforced Concrete Frames. *JOURNAL OF STRUCTURAL ENGINEERING* © ASCE. August 2002.
- [3] Kakaletsis DJ, Karayannis CG. Influence of Masonry Strength and Openings on Infilled R/C Frames Under Cycling Loading. *Journal of Earthquake Engineering*. 2008.
- [4] Tasnimi AA, Mohebbkhan A. Investigation on the behavior of brick-infilled steel frames with openings, experimental and analytical approaches. *Engineering Structures*. 2011;33:968-80.
- [5] Ozsayin B, Yilmaz E, Ispir M, Ozkaynak H, Yuksel E, Ilki A. Characteristics of CFRP retrofitted hollow brick infill walls of reinforced concrete frames. *Construction and Building Materials*. 2011;25:4017-24.
- [6] Altin S, Anil Ö, Kara ME, Kaya M. An experimental study on strengthening of masonry infilled RC frames using diagonal CFRP strips. *Composites Part B: Engineering*. 2008;39:680-93.
- [7] Erdem I, Akyuz U, Ersoy U, Ozcebe G. An experimental study on two different strengthening techniques for RC frames. *Engineering Structures*. 2006;28:1843-51.
- [8] Yuksel E, Ozkaynak H, Buyukozturk O, Yalcin C, Dindar AA, Surmeli M, et al. Performance of alternative CFRP retrofitting schemes used in infilled RC frames. *Construction and Building Materials*. 2010;24:596-609.
- [9] Chen W-W, Yeh Y-K, Hwang S-J, Lu C-H, Chen C-C. Out-of-plane seismic behavior and CFRP retrofitting of RC frames infilled with brick walls. *Engineering Structures*. 2012;34:213-24.
- [10] Agency FEM, Engineers ASOC. FEMA 356. Prestandard and commentary for the seismic rehabilitation of boudings: FEDERAL EMERGENCY MANAGEMENT AGENCY-Washington, D.C.; 2000.
- [11] Fiore A, Netti A, Monaco P. The influence of masonry infill on the seismic behaviour of RC frame buildings. *Engineering Structures*. 2012;44:133-45.
- [12] Asteris PG, Giannopoulos IP, Chrysostomou CZ. Modeling of Infilled frames with openings. *The Open Construction and Building Technology Journal*. 2012;M6:81-91.
- [13] Alam MS, Nehdi M, Amanat KM. Modelling and analysis of retrofitted and un-retrofitted masonry-infilled RC frames under in-plane lateral loading. *Structure and Infrastructure Engineering*. 2009;5:71-90.
- [14] D'Ayala D, Worth J, Riddle O. Realistic shear capacity assessment of infill frames: Comparison of two numerical procedures. *Engineering Structures*. 2009;31:1745-61.
- [15] Doudoumis IN. Finite element modelling and investigation of the behaviour of elastic infilled frames under monotonic loading. *Engineering Structures* 29 (2007) 1004–1024. 2007.
- [16] Asteris PG. Finite element micro-modeling of Infilled frames. *Electronic Journal of Structural Engineering*. 2008.
- [17] Asteris PG, Kakaletsis DJ, Chrysostomou CZ, Smyrou EE. Failure modes of in-filled frames. *Electronic Journal of Structural Engineering* 11(1) 2011. 2011.
- [18] Nwofor TC, Chinwah JG. Finite element modeling of shear strength of Infilled frames with openings. *International Journal of Engineering and Technology*. 2012;Volume 2 No. 6.
- [19] Nwofor TC. Numerical micro-modeling of masonry in filled frames *Scholars Research Library-Archives of Applied Science Research (Nigeria)*. 2012;4 (2):764-771.
- [20] Mohyeddin A, Goldsworthy HM, Gad EF. FE modelling of RC frames with masonry infill panels under in-plane and out-of-plane loading. *Engineering Structures*. 2013;51:73-87.
- [21] Dehghani A, Nateghi-Alahi, Fischer F. Engineered cementitious composites for strengthening masonry infilled reinforced concrete frames. *Engineering Structures*. 2015;105:197–208.
- [22] Erol, Karadogan G, Faruk H. Seismic strengthening of infilled reinforced concrete frames by CFRP Composites: Part B. *Engineering Structures*. 2016;91:473–91.
- [23] KAKALETSIS DJ. Comparison of CFRP and Alternative Seismic Retrofitting Techniques for Bare and Infilled RC Frames. *Journal of Composites for Construction*. 2011;15.
- [24] Pityzogia Aea. Strengthening of Infilled Reinforced Concrete Frames with TRM: Study on the Development and Testing of Textile-Based Anchors. *Journal of Composites for Construction*. 2014;18.
- [25] Bousias, al. SNe. Experimental Investigation of Concrete Frames Infilled with rc for Seismic Rehabilitation. *JOURNAL OF STRUCTURAL ENGINEERING* © ASCE. 2014;140.
- [26] Akin, Emre. Effects of Various Parameters on CFRP Strengthening of Infilled RC Frames'. *Journal of Performance of Constructed Facilities*. 2016;30.
- [27] Binici, al. Be. Numerical Study on CFRP Strengthening of Reinforced Concrete Frames with Masonry Infill Walls. *Journal of Composites for Construction*. 2014;18.
- [28] system Sos. Abaqus/CAE User's Manual.

- [29] 318 AC. Building code requirements for structural concrete and commentary (ACI 318-99). Detroit (MI): American Concrete Institute. 1999.
- [30] Saenz L. Discussion of “Equation for the stress-strain curve of concrete” by Desayi P, Krishnan S. ACI Journal. 1964.
- [31] Obaidat YT, Heyden S, Dahlblom O. The effect of CFRP and CFRP/concrete interface models when modelling retrofitted RC beams with FEM. Composite Structures. 2010.
- [32] Abaqus analysis user manual.
- [33] Sakr MA. FE modeling of simply supported RC beams strengthened with FRP plates Structural Faults & Repair, 13th International Conference, Edinburgh – UK. June 2010.
- [34] Obaidat YT, Heyden S, Dahlblom O, Farsakh GA-, Yahia, Abdel-Jawad. Retrofitting of reinforced concrete beams using composite laminates. Construction & Building Materials. 2010.
- [35] Brena SF, McGuirk GN. Advances on the Behavior Characterization of FRP-Anchored Carbon Fiber-Reinforced Polymer (CFRP) Sheets Used to Strengthen Concrete Elements. International Journal of Concrete Structures and Materials. March 2013;Vol.7, No.1:pp.3–16.
- [36] Niemitz CW, James R, Brena SF. Experimental behavior of carbon fiber-reinforced polymer (CFRP) sheets attached to concrete surfaces using CFRP anchors. Journal of Composites for Construction. 2010;14(2):185–94.